PRAMANA
— journal of
physics

Vol. 82, No. 5
May 2014
pp. 919–930

Dynamics of light, intermediate, heavy and superheavy nuclear systems formed in heavy-ion collisions

MANOJ K SHARMA* and GURVINDER KAUR
School of Physics and Materials Science, Thapar University, Patiala 147 004, India
*Corresponding author. E-mail: msharma@thapar.edu

DOI: 10.1007/s12043-014-0744-3; ***e*Publication:** 1 May 2014

Abstract. The dynamical description of light, intermediate, heavy and superheavy nuclei formed in heavy-ion collisions is worked out using the dynamical cluster decay model (DCM), with reference to various effects such as deformation and orientation, temperature, angular momentum etc. Based on the quantum mechanical fragmentation theory (QMFT), DCM has been applied to understand the decay mechanism of a large number of nuclei formed in low-energy heavy-ion reactions. Various features related to the dynamics of competing decay modes of nuclear systems are explored by addressing the experimental data of a number of reactions in light, intermediate, heavy and superheavy mass regions. The DCM, being a non-statistical description for the decay of a compound nucleus, treats light particles (LPs) or equivalently evaporation residues (ERs), intermediate mass fragments (IMFs) and fission fragments on equal footing and hence, provides an alternative to the available statistical model approaches to address fusion–fission and related phenomena.

Keywords. Dynamical cluster decay model; compound nucleus; heavy-ion reactions; deformations and orientations.

PACS Nos 24.10.−i; 25.70.Jj; 25.70.Gh

1. Introduction

In order to explore the hidden aspects of nuclear dynamics, a large amount of work has been done at both theoretical and experimental grounds since the last few decades. These efforts have provided solutions to many problems, but a significant number of associated nuclear features still need to be explored. The study of heavy-ion reactions, involving projectiles heavier than α-particle is of tremendous importance as it provides clues to the problems of nuclear structure and offers a testing ground for concepts related to nuclear forces. In low-energy regime, study of such reactions provides possibilities to examine nuclear structure and dynamical features associated with them.

The nuclei involved in a reaction may either be spherical or deformed having substantial distortions as compared to spherical shapes. There lies a possibility that either the

projectile or the target is deformed or there may also be the case of doubly deformed system where both the projectile and the target nuclei are deformed. As a result, it becomes extremely important to investigate the role of deformations and its effect on formation and decay processes of a compound nucleus (CN). In addition to deformations, significant role is played also by respective orientations of the projectile and the target at the time of nuclear collision and that of decaying fragments when the CN is on the verge of collapse. As the compound nuclear system finds itself in the excited state, the proper inclusion of temperature, excitation energy and angular momentum effects become indispensable. Thus, a theoretical model is required that incorporates these features and also accounts well for various decay processes so as to provide sufficient information about the dynamics of heavy-ion reactions.

Interestingly, the dynamical cluster decay model (DCM) of Gupta and collaborators [1–7], based on quantum mechanical fragmentation theory (QMFT) efficiently provides valuable information related to nuclear structure and reaction dynamics. It treats all the decay processes (i.e., light particles (LPs) or equivalently evaporation residues (ERs) ($Z_2 \leq 2$, $A_2 \leq 4$), intermediate mass fragments IMFs ($5 \leq A_2 \leq 20$) and fission fragments) on equal footing as dynamic collective mass motion of preformed clusters or fragments through the barrier and hence carries a distinct advantage over available statistical models. In addition to this, other important features of DCM are: (i) it takes into account the temperature-dependent binding energies [8], (ii) the deformation and orientation effects are duly incorporated, (iii) the barrier modification is an in-built feature of DCM due to the inclusion of neck-length parameter $\triangle R$ [9].

The orientation degree of freedom holds equal importance as that of deformations, and the same is investigated in DCM through hot 'equatorial' and cold 'polar' configurations [5,10]. In general, for deformed targets there lies a possibility that the projectile may hit the 'equatorial' region of the deformed target and hence form the most 'compact' configuration in its way to compound nucleus formation. It must be noted that hot 'equatorial' compact configuration corresponds to the smallest interaction radius and highest barrier height, while the cold 'polar' elongated orientation is used for the largest interaction radius and lowest barrier height. It must be noted that in QMFT-based calculations, hot configuration is preferred for ER, IMF and fusion–fission process and cold configuration is preferred for spontaneous fission, α-decays and cluster radioactivity.

In this paper, DCM is applied to study the decay processes of various nuclei. In addition to decay study of compound nucleus (CN), i.e., a composite system equilibrated in all degrees of freedom, the decay of other competing processes is also explored. DCM has been successfully applied to quasifission process in many systems. However, the work in this paper is confined to the study of compound nucleus decay and incomplete fusion (ICF) processes only. This paper is organized as follows. The DCM for hot and rotating compound nucleus including effect of deformations and orientations is briefly discussed in §2. Application of DCM to nuclei of various mass regions, and the results obtained are presented in §3. The conclusions drawn are summarized in §4.

2. The dynamical cluster-decay model (DCM)

In DCM [1–7], the decay of a hot and rotating nuclear system is studied as the dynamical collective clusterization process for the emission of light particles (LPs) or equivalently

evaporation residues (ERs), intermediate mass fragments (IMFs) and fission fragments. It is worked out in terms of the collective coordinates of mass (and charge) asymmetries $\eta = (A_1 - A_2)/(A_1 + A_2)$ (and $\eta_Z = (Z_1 - Z_2)/(Z_1 + Z_2)$), the relative separation R, the multipole deformations $\beta_{\lambda i}$ ($\lambda = 2, 3, 4$) and orientations θ_i ($i = 1,2$) of two nuclei or fragments (1 and 2 stand, respectively, for heavy and light fragments). In terms of these coordinates, for ℓ-partial waves, the compound nucleus decay cross-section is given by

$$\sigma = \frac{\pi}{k^2} \sum_{\ell=0}^{\ell_{\max}} (2\ell + 1) P_0 P; \qquad k = \sqrt{\frac{2\mu E_{\text{c.m.}}}{\hbar^2}}. \tag{1}$$

Here preformation probability P_0 refers to η motion and the penetrability P to R motion, both depending on angular momentum ℓ and temperature T. Also, $\mu = [A_1 A_2/(A_1 + A_2)]m$ is the reduced mass, with m as the nucleon mass and $\ell_{\max}$ is the maximum angular momentum which is fixed for the vanishing of the fusion barrier of incoming channel η_i or light particle cross-section $\sigma_{\text{LP}} \to 0$. The temperature T is related to CN excitation energy as $E^*_{\text{CN}} = [(A_{\text{CN}}/a)T^2 - T]$ with level density parameter $a = 9{-}11$. P_0 in eq. (1) is calculated by solving stationary Schrödinger equation in η, at a fixed $R = R_a$,

$$\left\{ -\frac{\hbar^2}{2\sqrt{B}_{\eta\eta}} \frac{\partial}{\partial \eta} \frac{1}{\sqrt{B}_{\eta\eta}} \frac{\partial}{\partial \eta} + V(R, \eta, T) \right\} \psi^v(\eta) = E^v \psi^v(\eta), \tag{2}$$

where $v = 0$, 1, 2, 3 refers to ground ($v = 0$) and excited state solutions, with ground state P_0 given as

$$P_0 = |\psi_R(\eta(A_i))|^2 \sqrt{B_{\eta\eta}} \frac{2}{A_{\text{CN}}}. \tag{3}$$

The mass parameters $B_{\eta\eta}$ are the smooth hydrodynamical masses [11]. The missing nuclear structure information of the CN in statistical models enters in DCM via the preformation probability P_0 of the fragments. For the competing ICF process, a part of the projectile interacts with target, and so P_0 is calculated in the same way as that for CN process, the only difference being that ICF leads to different composite systems depending on the break-up of the projectile nucleus. On the contrary, P_0 is taken as unity for quasi-fission (QF) process as the incoming channel keeps its identity intact in decay path. The QF results are not discussed in this paper.

The penetration probability P in eq. (1) is calculated using the WKB integral as

$$P = \exp\left(-\frac{2}{\hbar} \int_{R_a}^{R_b} \{2\mu[V(R) - Q_{\text{eff}}]\}^{1/2} \mathrm{d}R \right). \tag{4}$$

For the decay of a hot CN, R_a, the first turning point of the penetration path(s), used for calculating the penetrability P, is

$$\begin{aligned} R_a &= R_1(\alpha_1, T) + R_2(\alpha_2, T) + \Delta R(T) \\ &= R_t(\alpha, T) + \Delta R(T) \end{aligned} \tag{5}$$

with radius vectors

$$R_i(\alpha_i, T) = R_{0i}(T) \left[1 + \sum_{\lambda} \beta_{\lambda i} Y_{\lambda}^{(0)}(\alpha_i) \right]$$

and T-dependent nuclear radii R_{0i} of the equivalent spherical nuclei $R_{0i}(T) = [1.28A_i^{1/3} - 0.76 + 0.8A_i^{-1/3}](1 + 0.0007T^2)$ [12].

The potential $V(R, \eta, T)$, which goes as input in eq. (2) is defined as

$$V(R,\eta,T) = \sum_{i=1}^{2}[V_{\rm LDM}(A_i, Z_i, T)] + \sum_{i=1}^{2}[\delta U_i]\exp(-T^2/T_0^2) + V_C(R, Z_i, \beta_{\lambda i}, \theta_i, T) + V_P(R, A_i, \beta_{\lambda i}, \theta_i, T) + V_\ell(R, A_i, \beta_{\lambda i}, \theta_i, T). \quad (6)$$

Here, $V_{\rm LDM}$ is the T-dependent liquid-drop energy of Davidson *et al* [13] and δU is the 'empirical' shell correction, from Myers and Swiatecki [14], also made T-dependent to vanish exponentially with $T_0 = 1.5$ MeV [15]. V_P, V_C and V_ℓ are, respectively, the T-dependent, nuclear proximity, Coulomb and angular momentum ℓ-dependent potentials for deformed, oriented nuclei (for details, see [10]).

The neck-length parameter $\Delta R(T)$ in eq. (5) is the only parameter of the model used to fit the available experimental data. It allows us to define, equivalently, the 'barrier lowering' parameter ΔV_B, which simply relates $V(R_a, \ell)$ and the top of the barrier $V_B(\ell)$, for each ℓ,

$$\Delta V_B(\ell) = V(R_a, \ell) - V_B(\ell). \quad (7)$$

The barrier modification is quite useful for addressing the data at below barrier energies.

3. Results and discussions

In the framework of DCM, the dynamics of the reactions formed in heavy-ion collisions, leading to the formation of CN have been studied over a wide range of mass region. In this section, we have addressed the decay processes involved in different composite systems and the roles of deformation, orientation, angular momentum and excitation energy are duly investigated. The calculations were done using spherical choice of fragmentation and with the inclusion of quadrupole (β_{2i}) and hexadecapole ($\beta_{2i} - \beta_{4i}$) deformations. The results showing the above-mentioned effects, were illustrated in the form of fragmentation potential and preformation probability to extract information about various decay mechanisms present in light, intermediate, heavy and superheavy mass regions. The ICF process observed due to the involvement of loosely bound projectiles is also investigated in the framework of DCM. Depending on the mass of CN studied, this section is divided into four subsections namely, light mass nuclei, intermediate mass nuclei, heavy mass nuclei and superheavy nuclei.

3.1 *Light mass nuclei*

According to the study carried out using the rotating liquid-drop model (RLDM) it was expected that in very light mass compound nuclei with $A_{\rm CN} \sim 30$, the fusion–fission process is inhibited. However, some attempts have been made to explore the possibility of fusion–fission in light mass nuclear systems. One such attempt was made by Anjos *et al* [16] in an experiment carried out for studying the fission cross-sections in ^{28}Al* formed

in ^{18}O+^{10}B reaction and the same has been tested using DCM. Interestingly, ^{28}Al* is the lightest nucleus studied in the framework of DCM. We have fitted the data for fission fragments with Z=3, 4, 5, 6 using only the parameter of DCM, the neck-length parameter ΔR, and the calculated cross-sections find good agreement with the measured fission cross-sections. Figure 1 shows the fission cross-sections obtained using DCM and their comparison with available data at different excitation energies ($E_{\rm CN}$). It is worth mentioning that the neck-length parameter ΔR (see eq. (5)), is a measure of relative separation between two decaying fragments and assimilates the neck-formation effects [17]. This criterian is similar to the one adopted in two-centre shell model (TCSM). Interestingly, its magnitude is limited within 2 fm so as to justify the use of proximity interaction in DCM-based calculations. Figure 1 clearly signifies the importance of neck-length parameter ΔR in DCM calculations. At the touching configuration, i.e., $\Delta R = 0$ fm, the fission cross-sections were grossly underestimated at all energies. However, with the inclusion of appropriate ΔR, the DCM-based fission cross-sections perform better than the TSM results and find a good comparison with the measured fission cross-sections. A part of this result was presented in [18].

After studying the lightest compound system ^{28}Al* using DCM, we employed this methodology to ^{66}As*, which was formed in proton-halo ^{8}B induced reaction [19]. The study of its decay has been carried out at different energies lying across the Coulomb barrier. Interestingly, the decay study for this system includes contribution of LPs or equivalently ERs, intermediate mass fragments (IMFs) and fission fragments. It must be noted that ^{28}Al* being a relatively lighter system, was studied using spherical fragmentation approach only. However, for ^{66}As* the role of deformation of decaying fragments

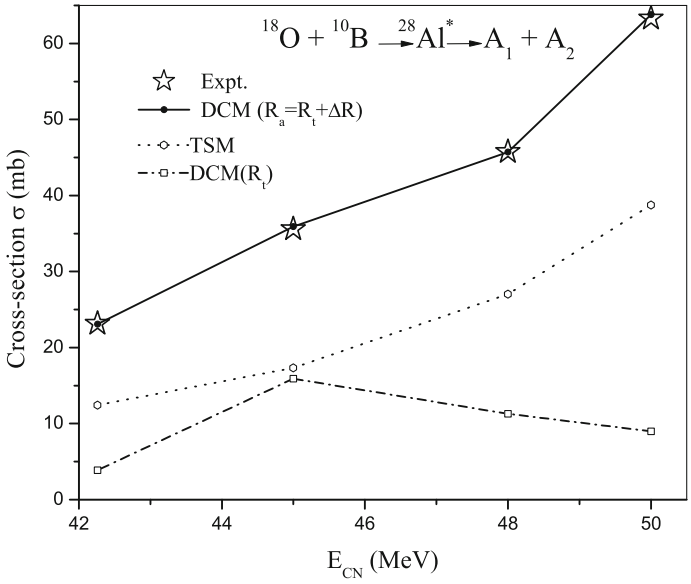

Figure 1. Comparison of fission cross-sections calculated using DCM with the experimental data.

was studied by taking into account spherical, quadrupole (β_{2i}) deformed and hexadecapole ($\beta_{2i} - \beta_{4i}$) deformed choice of fragmentation. For deformations $\beta_{\lambda i}$, we have taken β_{2i} and β_{4i} from [20] and the optimum orientations θ_i^{opt} of the hot fusion process for β_{2i} choice of fragmentation from [10]. However, for higher multipole deformations, i.e., β_{3i}, β_{4i} etc., the optimum orientation criteria do not work and hence, one needs to incorporate compact orientation approach as discussed in [21]. The calculations were carried out for all the three approaches using only the parameter of the model, neck-length parameter ΔR. In figure 2, the decay barrier height V_B is plotted as a function of fragment mass A_2 for $^8\text{B} + {}^{58}\text{Ni} \rightarrow {}^{66}\text{As}^*$ reaction and for all the three approaches i.e., spherical, quadrupole (β_{2i}) deformed and hexadecapole ($\beta_{2i} - \beta_{4i}$) deformed choice of fragmentation. It can be seen from figure 2 that decay barrier height (V_B) increases with increase in angular momentum, being maximum for $\ell_{\max}$. This trend is observed for all choices of fragmentation. For lower ℓ-values, V_B decreases with decrease in fragment mass (A_2), and hence, the decay probability for ER increases. On the contrary, at $\ell = \ell_{\max}$, V_B increases with decrease in fragment mass (A_2), particularly in ER region, thus favouring the emission of IMFs and fission fragments more in comparison to ERs. One may note that at $\ell = \ell_{\max}$, the barrier (decay) height is minimum for spherical fragmentation as compared to deformed fragmentation. This observation seems to suggest that for spherical fragmentation, probability of decay is more compared to quadrapole (β_{2i}) and hexadecapole ($\beta_{2i} - \beta_{4i}$) deformed choices. Interestingly, this reaction is not a pure compound nucleus reaction as the possible contribution from ICF channel may not be ruled out. In order to understand the behaviour of this reaction further, we have studied the fusion cross-section of ^{7}Be, originating through the break-up of ^{8}B ($^8\text{B} \rightarrow {}^7\text{Be} + p$) with

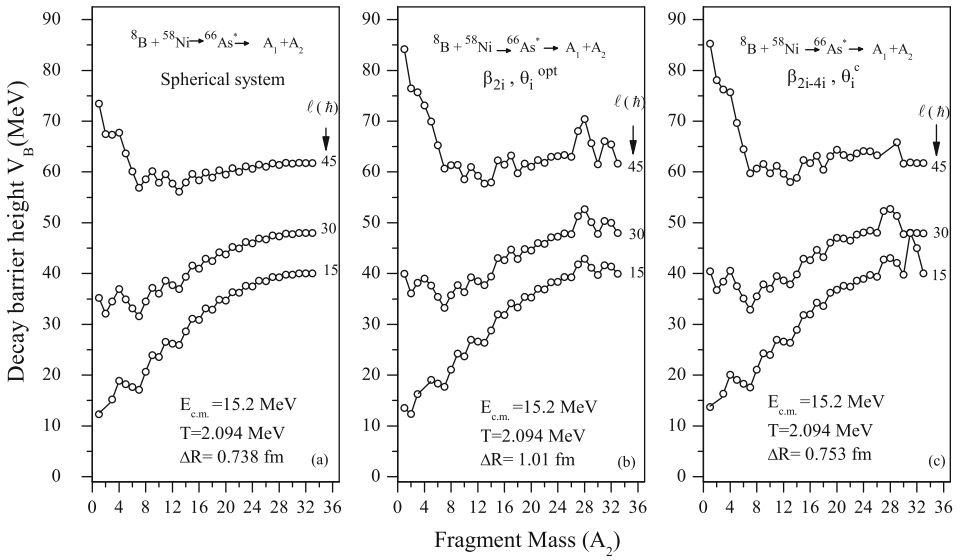

Figure 2. The decay barrier height for the decay of ^{66}As* into evaporation residues (ER), intermediate mass fragments (IMFs) and fission fragments calculated at different ℓ-values.

^{58}Ni target in reference to data of [22], by taking the quadrupole (β_{2i}) deformation into account. Corresponding to $E_{\rm lab} = 25.8$ MeV of ^{8}B, the $E_{\rm lab}$ for ^{7}Be obtained after energy correction [23,24] is 22.5 MeV with $E_{\rm c.m.} = 20.1$ MeV ($T = 2.23$ MeV). The variation of fragmentation potential, V (MeV), as a function of fragment mass (A_2) is shown for ^{8}B and ^{7}Be channels, respectively in figures 3a and 3b. The relative contribution of ERs, IMFs and fission fragments is almost identical for ^{8}B and ^{7}Be channels. A closer look at figure 3 suggests that the fragmentation path is almost identical in both cases except for the fact that α-nuclear structure starts vanishing at higher ℓ-values for ^{7}Be channel.

3.2 *Intermediate mass nuclei*

With an aim to understand the dynamics of intermediate mass nuclei, we have studied the fragmentation behaviour of ^{112}Xe* compound nucleus formed in ^{58}Ni+^{54}Fe reaction. Figure 4a, showing the variation of fragmentation potential as a function of fragment mass A_2, clearly depicts that at $\ell = 0\hbar$, β_{2i} deformation effects are silent, whereas they play a significant role in the fragmentation process at higher ℓ-values. At extreme ℓ-values, the α- nucleus structure is prominent for ER and IMF regions, which otherwise start vanishing in the fission region for spherical as well as the deformed choice of fragmentation. It is evident from figure 4a that $\ell_{\rm max}$ increases by a couple of units with the inclusion of deformation effects.

Another CN investigated for analysing the behaviour of intermediate mass fragment is the lanthanide system ^{158}Tb*, for which the complete fusion cross-section has a major

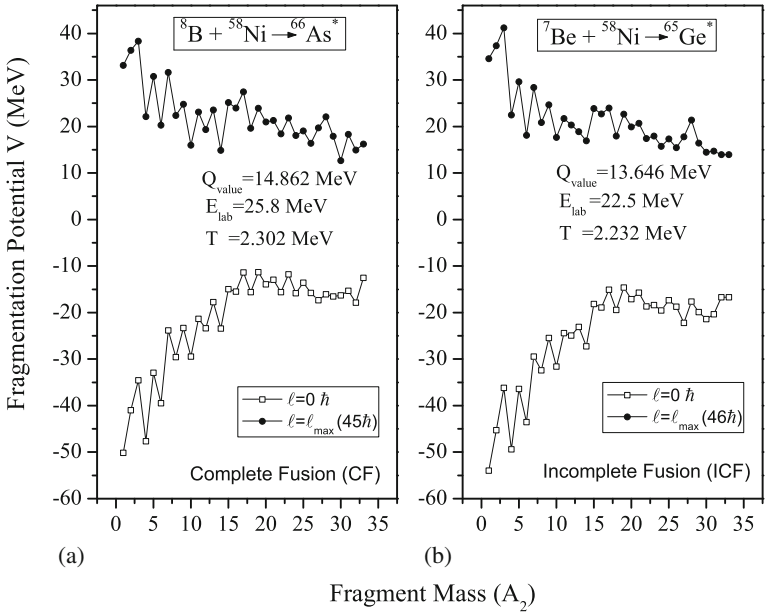

Figure 3. Variation of fragmentation potential $V(\eta)$ for fragments formed in (**a**) ^{8}B + ^{58}Ni and (**b**) ^{7}Be + ^{58}Ni reactions.

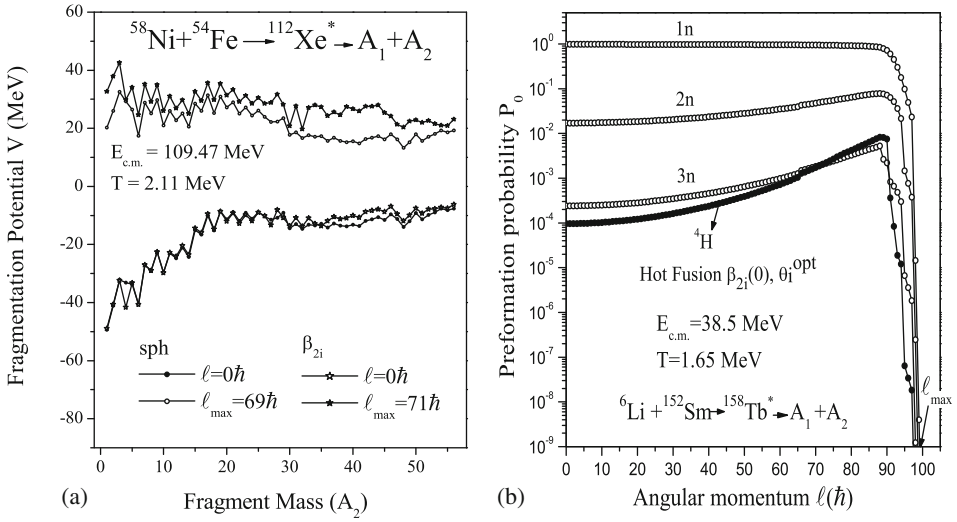

Figure 4. (**a**) Fragmentation potential V (MeV) as a function of fragment mass A_2 for ^{58}Ni +^{54} Fe $\rightarrow$^{112}Xe* reaction. (**b**) Preformation probability P_0 as a function of angular momentum $\ell(\hbar)$ for individual fragments contributing towards the decay of ^{158}Tb* system.

contribution through evaporation residue (σ_{ER}) while the fission cross-sections are almost negligible [25]. Hence, we have shown results pertaining to ER only. Interestingly, in the experiment at higher energies the contribution of charged particle is indicated but not identified. The DCM-based calculations identify the charged particle involved and its contribution in the ER decay is also accessed. Figure 4b illustrates the preformation probability P_0 as a function of angular momentum $\ell(\hbar)$ for individual fragments contributing towards the ER cross-section. It is relevant to mention here that in DCM-based calculations the minimum potential V (MeV) corresponds to the maximum preformation probability (P_0) and hence the maximum decay probability. The figure also reveals that the fragment with $A = 1$, i.e., $1n$ is preformed strongly, followed by $2n$, $3n$ and charged particle ^{4}H. Dynamics of ^{158}Tb* was investigated in our recent publication [26].

3.3 *Heavy mass nuclei*

Although the most probable decay mode for heavy nuclei is fission, a significant contribution from other decay channels such as ER may also be observed. We have investigated a large number of nuclear systems in heavy mass region $A_{CN} \sim 200$ [27], and systematic studies have been carried out to look for possible contribution of ER and fission processes. However, in this paper we present our results on ^{201}Bi* system formed in ^{20}Ne + ^{181}Ta reaction. This nuclear system is interesting as significant contribution of ICF process is also observed in this reaction due to the break-up of the projectile before complete amalgamation with target nucleus. The presence of ICF component makes nuclear

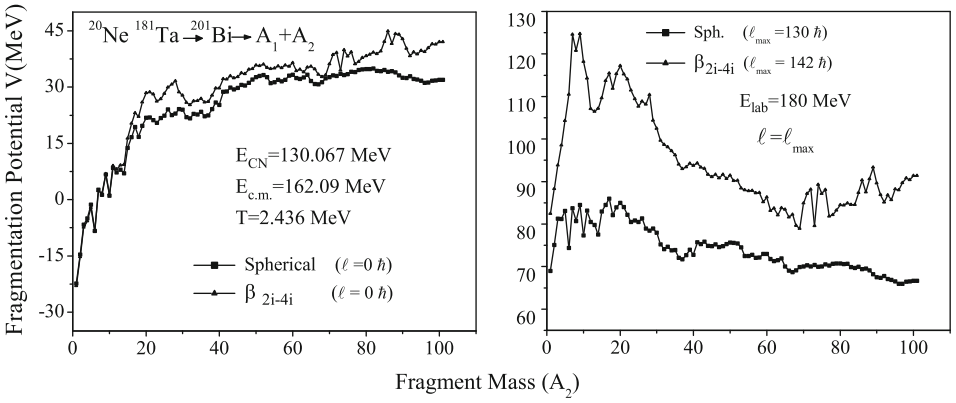

Figure 5. Variation of fragmentation potential as a function of fragment mass (A_2) for decay of ^{201}Bi* nucleus at $E_{\rm lab} = 180$ MeV.

reaction dynamics more informative and interesting as far as nuclear structure and related phenomena are concerned. In this section, we discuss the effect of hexadecapole deformations along with the ICF component observed in ^{20}Ne + ^{181}Ta reaction. From figure 5, showing variation of fragmentation potential with fragment mass A_2 at higher energy, i.e., $E_{\rm lab}$=180 MeV, a significant effect of deformations is evident at extreme ℓ-values, being more prominent at ℓ=$\ell_{\rm max}$. In ^{201}Bi* system, in addition to ER, contribution from ICF is also observed due to the break-up of ^{20}Ne projectile into four dominant channels, i.e., ^{4}He, ^{8}Be, ^{14}N and ^{16}O transfer channels. As mentioned earlier, a suitable energy correction is applied to account for the observed ICF contribution. The fractional ICF contribution of each transfer channel towards total cross-section is observed to be the most for ^{4}He transfer channel, followed by ^{8}Be, ^{14}N, ^{16}O transfer channels. This implies that ICF cross-section of ^{201}Bi* is more for mass asymmetric channel, which is in line with the systematics of Morgenstern [28]. Part of these results are published in [23].

3.4 *Superheavy nuclei*

The overall attempt to study nuclear dynamics in different mass regions would be incomplete without the involvement of superheavy nuclei. After studying the indispensable role of quadrupole and hexadecapole deformations, angular momentum and temperature in light, intermediate and heavy mass nuclei, calculations were done to observe the effect of orientations in the decay of ^{268}Sg* nucleus and the role of quadrupole β_{2i} deformations in ^{286}112*. At below barrier there lies a possibility that the projectile may hit the deformed target in 'polar' region giving rise to 'elongated' configuration, whereas at above barrier energies the equatorial orientation is preferred thus forming 'compact' configuration. Figures 6a and 6b show variation of preformation probability P_0 as a function of fragment mass, for the decay of ^{268}Sg* nucleus formed in ^{30}Si + ^{238}U reaction for equatorial and polar configurations. It is observed that fission fragment distribution is symmetric at above barrier energy and becomes asymmetric at below barrier energy. In other words, it can be said that fragmentation changes from symmetric to asymmetric

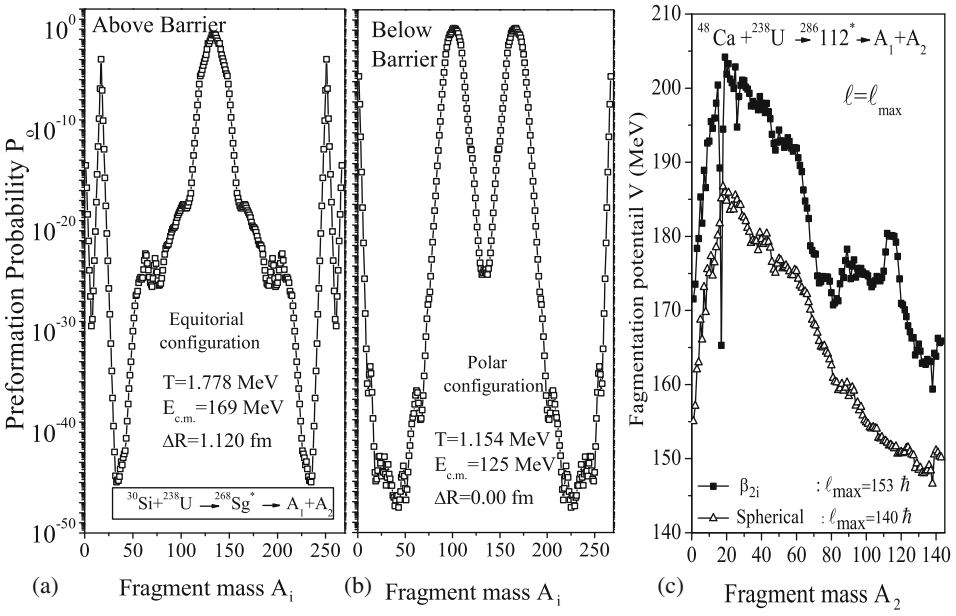

Figure 6. Variation of preformation probability P_0 as a function of fragment mass A_i, for the decay of ^{268}Sg* nucleus formed in ^{30}Si + ^{238}U reaction for (**a**) equatorial and (**b**) polar configuration. (**c**) Fragmentation potential for the decay of ^{286}112* nucleus formed in ^{48}Ca + ^{238}U reaction.

on going from above barrier (equatorial) to below barrier (polar) configurations. The asymmetric peaks at below barrier energy may be associated with some competing non-compound nucleus (nCN) mechanism. Decay of ^{268}Sg* was investigated in our recent publication [5]. Besides this, we have addressed the role of quadrupole deformations β_{2i} in ^{286}112* formed in ^{48}Ca + ^{238}U reaction. In figure 6c the fragmentation potential is plotted as a function of fragment mass for spherical and β_{2i} deformed choice of fragmentation. The potential energy surfaces (PES) are quite different for spherical and deformed choices of fragmentation particularly in heavy mass fragment (HMF) region. However, the fission fragment distribution is almost symmetric for spherical and deformed fragmentations.

4. Summary and conclusions

It is observed that for the lightest nucleus ^{28}Al*, DCM-based results find good agreement with the experimental fission cross-sections. Moreover, the results clearly signify the importance of neck-length parameter ΔR in DCM-based calculations. By studying the role of deformations in the next higher system ^{66}As*, it seems that for spherical fragmentation, the decay probability is more than that for deformed fragmentation. Also, at

$\ell=\ell_{\max}$, V_B is found to increase with the decrease in fragment mass as a result of which the emission of IMFs and fission fragments starts competing with ERs. The emission probability of ERs is consistently higher at lower ℓ-values. The possible contribution from ICF is also studied for this system and it is observed that like complete fusion, the contributing fragments for ICF are also the same, i.e., ERs, IMFs and fission fragments. The fragmentation path is almost identical in both cases but the α-nucleus structure starts vanishing at higher ℓ-values for ICF channel. Also, deformations are observed to play a significant role in the intermediate mass nucleus ^{112}Xe*, being more prominent at higher ℓ-values. The next higher intermediate system studied, ^{158}Tb* enlightens another feature of DCM, of identifying the missing charged particle and its contribution in ER decay. In the heavy mass nucleus ^{201}Bi*, the application of DCM with reference to ICF is observed once again through four dominant transfer channels. It is observed that contribution of ICF is maximum for mass asymmetric channel and decreases with decrease in mass asymmetry. After studying the role of deformations, the effect of orientation is observed in the superheavy nucleus ^{268}Sg*. It is observed that fission fragment distribution changes from symmetric to asymmetric on going from above to below barrier energies where the asymmetric peak may be associated with some nCN mechanism. Finally, the role of quadrupole deformation has been observed for $^{286}112^*$ system. The deformation, temperature and angular momentum effects are shown to influence the decay path of a variety of nuclear systems formed in different mass regions via heavy-ion reactions.

Acknowledgement

Thanks are due to Prof. R K Gupta and Ph.D. students Kirandeep Sandhu and Manpreet Kaur for their valuable contributions in this work.

References

[1] S S Malik and R K Gupta, *Phys. Rev. C* **39**, 1992 (1989)
[2] R K Gupta, S K Arun, R Kumar and Niyti, *Int. Rev. Phys. (IREPHY)* **2**, 369 (2008)
[3] B B Singh, M K Sharma and R K Gupta, *Phys. Rev. C* **77**, 054613 (2008)
[4] M K Sharma, G Sawhney, R K Gupta and W Greiner, *J. Phys. G* **38**, 105101 (2011)
[5] K Sandhu, M K Sharma and R K Gupta, *Phys. Rev. C* **86**, 064611 (2012)
[6] M Kaur, R Kumar and M K Sharma, *Phys. Rev. C* **85**, 014609 (2012)
[7] R K Gupta and W Greiner, in *Heavy elements and related new phenomenon* edited by W Greiner and R K Gupta (World Scientific, Singapore, 1999) Vol. I, Chap. 14, p. 536
[8] R K Gupta *et al*, *Phys. Rev. C* **68**, 014610 (2003)
[9] S K Arun, R Kumar and R K Gupta, *J. Phys. G* **36**, 085105 (2009)
[10] R K Gupta *et al*, *J. Phys. G* **31**, 631 (2005)
[11] H Kroger and W Scheid, *J. Phys. G* **6**, L85 (1980)
[12] G Royer and J Mignen, *J. Phys. G* **18**, 1781 (1992)
[13] N J Davidson *et al*, *Nucl. Phys. A* **570**, 61c (1994)
[14] W D Myers and W J Swiatecki, *Nucl. Phys. A* **81**, 1 (1966)
[15] A S Jensen and J Damgaard, *Nucl. Phys. A* **203**, 578 (1973)
[16] R M Anjos *et al*, *Phys. Rev. C* **48**, R2154 (1993); *Phys. Rev. C* **49**, 2018 (1994)

[17] S Kumar and R K Gupta, *Phys. Rev. C* **55**, 218 (1997)
[18] B B Singh *et al*, *Proceedings of DAE symposium on Nuclear Physics* **55** (2012)
[19] E F Aguilera *et al*, *Phys. Rev. Lett.* **107**, 092701 (2011)
[20] P Moller *et al*, *At. Data Nucl. Data Tables* **59**, 185 (1995)
[21] R K Gupta, M Manhas and W Greiner, *Phys. Rev. C* **73**, 054307 (2006)
[22] E F Aguilera *et al*, *Phys. Rev. C* **79**, 021601(R) (2009)
[23] G Kaur and M K Sharma, *Nucl. Phys. A* **884**, 36 (2012)
[24] P P Singh *et al*, *Phys. Rev. C* **77**, 014607 (2008)
[25] P K Rath *et al*, *Nucl. Phys. A* **874**, 14 (2012)
[26] G Kaur and M K Sharma, *Phys. Rev. C* **87**, 044601 (2013)
[27] M Kaur and M K Sharma, *Phys. Rev. C* **85**, 054605 (2012)
S Kanwar *et al*, *Int. J. Mod. Phys. E* **18**, 1453 (2009)
G Sawhney and M K Sharma, *Eur. Phys. J. A* **48**, 57 (2012)
[28] H Morgenstern *et al*, *Phys. Rev. Lett.* **52**, 1104 (1984)